

Reprint from

IAVCEI Proceedings in Volcanology, Vol. 2

Lava Flows and Domes

Edited by Jonathan Fink

© Springer-Verlag Berlin Heidelberg 1989

Printed in Germany. Not for Sale.

Reprint only allowed with permission from Springer-Verlag.



Springer-Verlag Berlin Heidelberg New York
London Paris Tokyo Hong Kong

Lava Domes Modeled as Brittle Shells that Enclose Pressurized Magma, with Application to Mount St. Helens

R. M. IVERSON

Abstract

Lava domes can be modeled mathematically as brittle shells that enclose pressurized magma. This chapter describes a static, brittle-shell model that is conceptually distinct from previous models of lava domes. The governing equations of the brittle-shell model embody several simplifying assumptions, none of which restricts the rheology of lava-dome constituents. The single morphologic assumption is that lava domes are axially symmetric. The most important mechanical assumption is that, in domes which are growing slowly and endogenously, stresses are in quasi-static equilibrium. This equilibrium may be disrupted by extrusions or explosions, which reflect transient adjustments that lead to a new equilibrium of the dome. The mechanical parameters included in the model are the thickness and tensile strength of the dome's outer shell and the unit weight and excess pressure of the enclosed magma and gas. These four parameters combine to form a single dimensionless number, D , which completely governs the equilibrium dome shape. The value of D is about one for the Mount St. Helens dome. Morphologic measurements on the Mount St. Helens dome show that its growth has been nearly self-similar since May 1981, and field observations show that failure of the dome's outer shell, accompanied by extrusions, has been an important growth process (Swanson and Holcomb, this Vol.). Theoretical predictions based on the brittle-shell model are consistent with both of these phenomena.

1 Introduction – The Conceptual Model

A lava dome is a steep-sided, rounded extrusion that forms a dome-shaped or bulbous mass of congealed lava above and around a volcanic vent (Bates and Jackson 1980). Quantifying and testing hypotheses about the physical processes that control the shape and growth of lava domes can improve understanding of eruptive mechanisms and hazards at volcanoes where domes exist.

This chapter describes formulation and testing of quantitative predictions based on the hypothesis that lava domes are essentially two-component systems in static or quasi-static mechanical equilibrium. One component of the system is an internal body of ductile magma, and the other component is an external shell or carapace of solid, brittle rock (Fig. 1). When forces in the two components of the system are balanced in static equilibrium, the system resides in a state of minimum free energy. Nonequilibrium states of the system, which occur during eruptive lava-dome growth, are transient phenomena that restore the system to a new state of equilibrium. Lava-dome growth consequently is regarded as a succession of static or quasi-static equilibrium states, which are punctuated by intermittent eruptions.

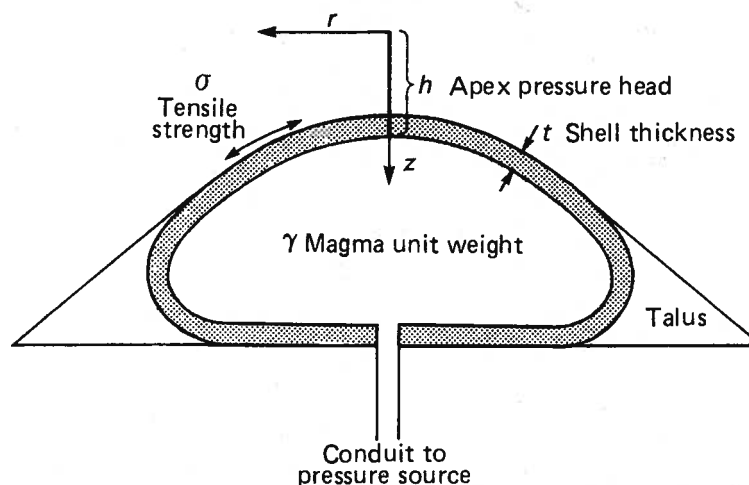


Fig. 1. Conceptual model of a lava dome viewed in cross-section. The parameters that play a role in the brittle-shell dome model are identified

Another component that might be considered part of the lava-dome system is a skirt or apron of talus around the dome (Fig. 1). Here the talus is assumed to be mechanically decoupled from the dome system. Thus, the talus can contribute to the external morphology of the dome, but it cannot contribute strength that affects the equilibrium of the dome. Although this assumption is not completely realistic, its use nevertheless appears warranted, owing both to its role in simplifying predictions and to the observation that talus surfaces generally slope at the angle of repose. Thus, any outward force that steepens the talus slopes will cause them to fail, and they will provide relatively little support for the growing dome carapace.

It also seems reasonable to assume that the dome's solid carapace and internal magma each are isothermal and homogeneous, and that the dome is axially symmetric. These assumptions are reasonable not because they are likely to apply exactly to lava domes, but because they lead to simple, unambiguous predictions that can be readily compared and contrasted to the behavior of lava domes.

Under the assumptions described above, the problem of predicting equilibrium dome configurations requires that only four physical parameters be considered. These are the tensile strength of the dome's solid carapace, σ ; the thickness of the carapace, t ; the unit weight of the fluid magma, γ ; and the pressure head, h ($= \text{pressure}/\gamma$) of the magma at the apex of the dome (Fig. 1). The analysis that follows this discussion shows that these four parameters combine to form a single dimensionless number, D , that governs equilibrium dome configurations.

None of the parameters that combine to form D embodies assumptions about rheology. The ductile magma within the dome can be linearly or nonlinearly viscous, and the solid rock carapace can be elastic or plastic, as long as the stress state departs insignificantly from equilibrium. Assumptions

about rheology are unnecessary because the problem of finding equilibrium dome configurations is statically determinate.

Equilibrium is regarded as a critical limiting state, and its role might be clarified by a simple thought experiment. At equilibrium the dome carapace is uniformly stressed; its strength just suffices to contain the magma pressure exerted from within. In other words, if σ , t , and γ are, for the moment, assumed to be constants, then an increase in h will be accommodated either by a change in equilibrium dome shape or by a non-equilibrium response such as tensile failure of the dome carapace, which would be accompanied by an extrusion or explosion. An extrusion or explosion changes the magma pressure and/or the properties of the dome carapace, resulting in a new state of equilibrium. Alternatively, quasi-equilibrium dome growth can occur continuously and endogenously if, for example, the thickness and/or strength of the solid carapace increases with time. The *rate* at which endogenous dome growth or eruptions occur depends on the dome-rock rheology and the subterranean magma pressure and supply rate, which are analyzed in an accompanying chapter (Denlinger 1987, and this Vol.).

Before considering the brittle-shell analysis in detail, it is worthwhile to note that the rheology of lava-dome constituents probably varies more or less continuously with distance from the center of the dome. Near the center, the magma may exist at temperatures high enough to ensure fully fluid behavior; complete stress relaxation probably occurs in tens of seconds (cf. Goetze 1971), and the magma probably flows in response to any deviatoric stress. Toward the dome exterior, the dome rock becomes progressively cooler and more solid. At the exterior surface it has considerable rigidity, and it can support some deviatoric stress almost indefinitely. The brittle-shell model idealizes this continuously varying system by treating it as a two-layer system. This idealization, although imperfect, can provide insights to dome behavior that are not provided by models that idealize lava domes as homogeneous, single-phase fluids or solids (e.g., Huppert et al. 1982).

2 Analysis

The analysis described here follows and builds upon the analysis of drop-shaped fluid storage tanks described by Flügge (1967, p. 1–45), and the reader is referred to Flügge's exhaustive treatment for further details. Drop-shaped storage tanks provide a close mechanical analog to the brittle-shell concept of lava domes, because in each case the tensile strength of an exterior carapace or shell constrains the shape of the pressurized fluid mass within.

Referring to the curvilinear, orthogonal coordinate system imposed on the curved shell segment pictured in Fig. 2, consider the system of stresses and stress resultants (which are forces per unit length of the surface upon which they act) in the shell. Normal- and shear-stress resultants that act in the plane of the shell are designated by N , and stress resultants that act transverse to the

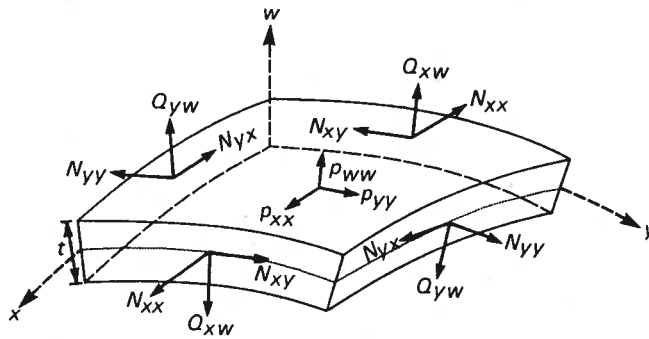


Fig. 2. A segment of the curved shell of a lava dome, showing the coordinate system and stress components

plane of the shell are designated by Q . The first subscript of each resultant in Fig. 2 designates the coordinate direction of the normal to the plane upon which it acts, and the second subscript designates its direction of action. In addition to the stress resultants N and Q , there is a stress, p , that acts through the centroid of the shell. This stress is caused by internal magma pressure and by the weight of the rock in the shell.

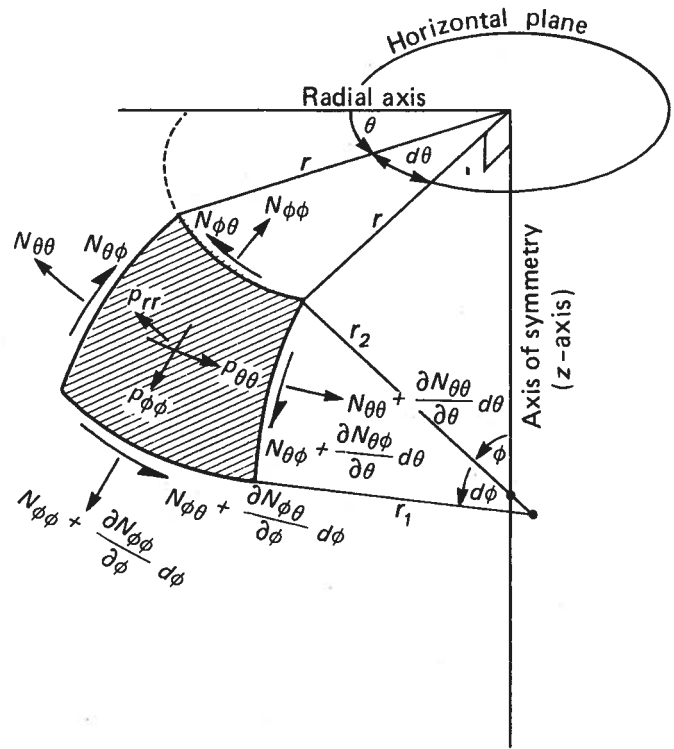
As described in detail by Flügge (1967), a remarkable simplification of the stress system shown in Fig. 2 is possible if some tenable assumptions are made. Assuming that no moment flexes the shell out of its equilibrium curvature, the stress resultants N_{xx} and N_{yy} must vary slightly with w just so as to preserve equilibrium. Similarly, assuming that no moment twists the shell, N_{yx} and N_{xy} must also vary with w just so as to preserve equilibrium. These assumptions appear reasonable, given that internal magma pressure is the only "external" force available to flex or twist the shell. At equilibrium, internal magma pressure varies linearly with depth and imposes no loads that distort the shell. The assumption of insignificant bending and twisting moments therefore appears good, and it is reasonable to neglect such moments.

A further simplification of the stress system shown in Fig. 2 arises from consideration of the moment equilibrium of surfaces in the x - y plane. First, there is equilibrium of such surfaces with respect to torsion about the w -axis only if $N_{xy} = N_{yx}$. Second, equilibrium of such surfaces with respect to torsion about the y -axis exists only if $Q_{xw} = 0$, and equilibrium with respect to torsion about the x -axis exists only if $Q_{yw} = 0$. This means that only the resultants designated by N and the stresses designated by p affect the balance of forces in the shell, and the analysis reduces to that of "membrane" forces (Flügge 1967).

In an analysis of membrane forces, the shell is replaced, in effect, by an infinitesimally thick membrane. Despite the fact that the shell has a finite thickness, t (Figs. 1 and 2), it can be modeled as a membrane (Fig. 3) with little loss in accuracy.

For convenience, now consider angular coordinates of the membrane, designated ϕ in the meridional direction and θ in the parallel direction (Fig. 3). The radial coordinate of the membrane, r , varies as some unknown function of ϕ and θ , and finding this function is the essence of the problem.

Fig. 3. The membrane model of the dome shell, showing the coordinate system and stress resultants. r_1 is the radius of curvature in the meridional direction; it is perpendicular to the shell surface but does not necessarily terminate on the axis of symmetry. r_2 is the radius of curvature in the parallel direction; it is perpendicular to the shell surface and terminates on the axis of symmetry



Balancing the force components in the membrane leads to force-equilibrium equations for the ϕ , θ , and r directions. For the meridional (ϕ) direction, equilibrium is expressed by

$$\frac{\partial}{\partial \phi} (r N_{\phi\phi}) + r_1 \frac{\partial N_{\theta\phi}}{\partial \theta} - r_1 N_{\theta\theta} \cos \phi + p_{\phi\phi} r r_1 = 0 ; \quad (1a)$$

and in the parallel (θ) direction, by

$$\frac{\partial}{\partial \phi} (r N_{\phi\theta}) + r_1 \frac{\partial N_{\theta\theta}}{\partial \theta} + r_1 N_{\phi\theta} \cos \phi + p_{\theta\theta} r r_1 = 0 ; \quad (1b)$$

and in the radial (r) direction, by

$$\frac{N_{\phi\phi}}{r_1} + \frac{N_{\theta\theta}}{r_2} = p_{rr} . \quad (1c)$$

For the somewhat lengthy derivation of Eqs. (1), the reader is referred to Flügge (1967). Definitions of the variables in these equations are illustrated in Fig. 3.

Because the dome is axially symmetric, all derivatives with respect to the parallel coordinate, θ , must vanish. Equations (1 a) and (1 b) thus reduce to

$$\frac{d}{d\phi} (rN_{\phi\phi}) - r_1 N_{\theta\theta} \cos \phi + p_{\phi\phi} r r_1 = 0 ; \quad (2a)$$

$$\frac{d}{d\phi} (rN_{\phi\theta}) + r_1 N_{\phi\theta} \cos \phi + p_{\theta\theta} r r_1 = 0 , \quad (2b)$$

where Eq. (2b) contains only the shear-stress resultant ($N_{\phi\theta}$) and is independent of Eqs. (2a) and (1c), which specify the normal-stress resultants ($N_{\phi\phi}$ and $N_{\theta\theta}$). Thus, Eq. (2b) is not needed to obtain the $r(\phi)$ or $\phi(r)$ solution.

The external load imposed on the membrane by the magma pressure acts normal to the membrane surface, because the liquid magma supports no shear stress. Moreover, the membrane approximation assumes that the body force caused by the weight of the rigid shell is negligible compared to the external (magma) load and its attendant reaction stresses. The stress p consequently has no component in the ϕ - or θ -directions, and is given simply by

$$p = p_{rr} = \gamma z , \quad (3)$$

where γ is the magma's unit weight, and z is a vertical coordinate with its origin ($z = 0$) at a height h above the apex of the dome. The coordinate z is reckoned positive downward (Fig. 1).

For an equilibrium shell of constant strength, σ , and thickness, t , the stress resultants $N_{\phi\phi}$ and $N_{\theta\theta}$ must by definition each equal σt . Using this fact and Eq. (3), Eq. (1c) reduces to

$$\sigma t (1/r_1 + 1/r_2) = \gamma z ; \quad (4)$$

and Eq. (2a) reduces to a simple geometric relation:

$$\sigma t (dr/d\phi - r_1 \cos \phi) = 0 . \quad (5)$$

Equations (4) and (5) contain only the variables ϕ , r , and z . However, they also contain the geometric parameters r_1 and r_2 , which need to be eliminated before solutions can be obtained.

The parameter r_2 is eliminated by expressing it in terms of the geometry of Fig. 3:

$$r_2 = r/\sin \phi , \quad (6)$$

and r_1 is eliminated by expressing it in terms of Eq. (5):

$$\frac{1}{r_1} = (\cos \phi) \frac{d\phi}{dr} = \frac{d}{dr} (\sin \phi) . \quad (7)$$

Substituting Eqs. (6) and (7) into Eq. (4) yields a differential equation that governs the shape of a meridian on the dome surface:

$$\frac{d(\sin \phi)}{dr} + \frac{\sin \phi}{r} = \frac{\gamma z}{\sigma t} . \quad (8)$$

This equation, however, contains both ϕ and z as undetermined functions of r . Thus, another differential equation, which is deduced from the geometry of Fig. 3, provides closure to Eq. (8) by relating ϕ , z , and r along a meridian:

$$\tan \phi = dz/dr . \quad (9)$$

Simultaneous solution of Eqs. (8) and (9) therefore yields ϕ and z as functions of r along a meridian; this relation completely determines the shape of the dome. The nonlinear system of Eqs. (8) and (9) is not tractable analytically, but is readily solved by elementary numerical methods.

To maximize the applicability of numerical solutions, it is useful to normalize or "scale" Eqs. (8) and (9) so that all their variables are dimensionless. To normalize the equations three dimensionless variables are introduced:

$$\varrho = r / \sqrt{\frac{\sigma t}{\gamma}} ; \quad \xi = z / \sqrt{\frac{\sigma t}{\gamma}} ; \quad \eta = \sin \phi . \quad (10 \text{ a, b, c})$$

Substituting Eqs. (10) into Eq. (8) then yields

$$\frac{d\eta}{d\varrho} = \xi - \frac{\eta}{\varrho} ; \quad (11)$$

and substituting Eqs. (10) into Eq. (9) yields

$$\frac{d\xi}{d\varrho} = \frac{\eta}{\sqrt{1-\eta^2}} , \quad (12)$$

so that there is a nonlinearly coupled pair of first-order, ordinary differential equations (11 and 12) to solve for the dependent variables η and ξ .

Note that the parameter $\sqrt{\sigma t/\gamma}$ appears prominently as the natural length scale in Eqs. (10), (11), and (12). Scaled against this reference length, points on the dome surface have the coordinates (ϱ, ξ) , where ϱ is the normalized radial distance from the dome axis and ξ is the normalized vertical distance below an origin that lies a distance h above the dome apex (Fig. 1). The distance h also can be scaled relative to the reference length $\sqrt{\sigma t/\gamma}$, yielding the dimensionless number

$$D = \sqrt{\frac{\sigma t}{\gamma}} / h . \quad (13)$$

This dimensionless number incorporates all the physical parameters that affect the shape of the dome, and it therefore governs the mathematical solution completely. That is, the solutions of Eqs. (11) and (12) comprise an orderly family, the members of which are distinguished only by their value of D .

The boundary conditions used to solve Eqs. (11) and (12) are found at the dome apex, where $r = 0$ and, in terms of the normalized variables, $\varrho = 0$. The boundary conditions are

$$\eta(\varrho = 0) = 0 ; \quad \xi(\varrho = 0) = h / \sqrt{\frac{\sigma t}{\gamma}} = 1/D . \quad (14a, b)$$

The first of these conditions is derived from the requirement that the dome-surface slope must be zero at the dome apex, and the second is derived from the requirement that, by definition, $z = h$ at the apex (Fig. 1).

Solving the system (11, 12, 14a, b) numerically requires relatively simple but rather unique tactics. The uniqueness arises out of difficulty in beginning the computation stably and out of a necessity to switch computational algorithms depending on whether $\sin \phi$ or $\cos \phi$ is in the neighborhood of zero. For details of these tactics, the reader is referred to the discussion by Flügge (1967). It is easy to implement Flügge's suggestions computationally and to solve the system of equations by using a numerical integration procedure. A user-friendly BASIC program called "Halfdome" (Appendix 1) solves the equations using a Runge-Kutta algorithm (Kreyszig 1979, p. 797) and plots the cross-sectional shape of half of an axially symmetric lava dome.

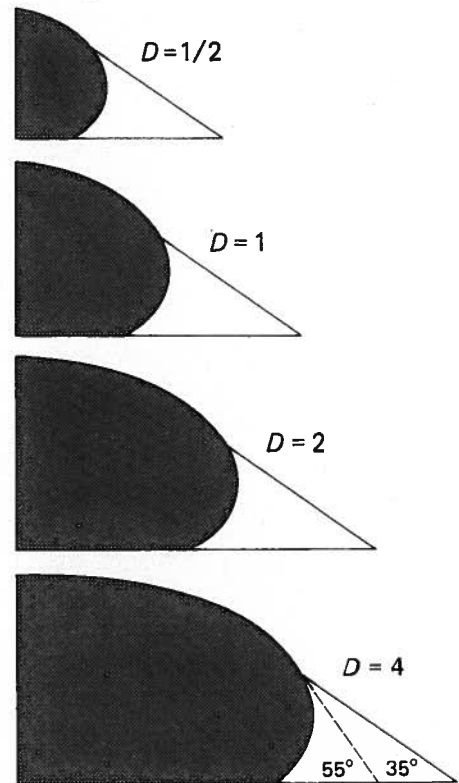
3 Solutions

Figure 4 shows a series of solutions generated by using "Halfdome". The solutions illustrate how the equilibrium shape and relative size of the dome change as a function of D , and additional solutions show the same trend over a much wider range of D . The talus aprons shown on the solutions in Fig. 4 adjoin the dome surface arbitrarily at the point where the slope angle is 55° , but the talus aprons themselves slope at an arbitrary angle of 35° . These angles are adjustable parameters that do not affect the solution of the equilibrium equations in "Halfdome" (Appendix 1).

4 Discussion

The model results described above constitute an hypothesis aimed at explaining the morphology and style of growth of lava domes. Here this hypothesis is compared with other quantitative hypotheses for lava-dome growth and with data collected at Mount St. Helens.

Fig. 4. A family of lava-dome cross-sectional profiles computed using "Halfdome". Profiles are shown for different values of D . The shaded part of each profile represents the dome shell and interior, and the unshaded part represents the bordering talus apron. The talus apron adjoins the shell at an arbitrary angle of 55° but slopes at an angle of 35°



4.1 Comparison with Other Hypotheses

Two quantitative hypotheses for the mechanical controls of lava-dome growth and morphology have been advanced previously. The first of these, by Huppert et al. (1982), postulates that lava domes behave like a pile of linearly viscous fluid. Fluid is continuously injected through the base of the pile to maintain the rotund shape of the lava dome. Thus, the lava dome cannot achieve a state of static equilibrium. It must constantly expand volumetrically; otherwise it sags into a flatter and flatter viscous pile. Measurable sagging of this type occurs between eruptions on the Mount St. Helens dome (D. A. Swanson, U.S. Geological Survey, personal communication), but the dome does not continue to sag indefinitely.

Another important feature of the Huppert et al. (1982) linear-viscous model is that fluid pressures within the dome are hydrostatic; there can be no buildup of excess pressure that could potentially cause an explosion, and there is no means of generating localized extrusions.

The key parameter in the linear-viscous model is the fluid or lava viscosity, which determines the shape of the lava dome and its rate of spreading. In order to achieve reasonable fits to the observed lava-dome shape at the Soufriere of St. Vincent volcano, Huppert et al. (1982) needed to use a lava viscosity of

2×10^{12} poise, which is several orders of magnitude larger than typical measured lava viscosities. Huppert et al. attributed their discrepant theoretical viscosity to the presence of a high-viscosity "skin" they observed on the outer surface of the dome but could not simulate with their uniform-viscosity model. The skin constrained the flow of the magma within the dome to such an extent that it effectively dominated the dome behavior.

A second hypothesis for the controls of lava-dome growth and morphology has been advocated by Blake (1987, and this Vol.), who models a dome as a pile of Bingham (viscoplastic) material. This material has a finite shear strength as well as viscosity, and Blake's model consequently appears to be more realistic than the linear-viscous model. However, it uses two key concepts that are identical to those of the linear-viscous model: (1) that the dome is a pile of homogeneous material, with properties in the outer shell that are identical to those in the dome interior; and (2) that fluid pressure in the dome is hydrostatic. The Bingham model is appealing in its ability to represent static, equilibrium dome states (this is rendered possible by the yield strength in the model), but the model admits strength only in shear, and not in tension. Blake obtained estimates of lava-dome yield strengths by using an equilibrium relationship between dome height, radius, density, and yield strength that he derived from small-scale model experiments using kaolin slurries. The relationship shows that the dome height is always proportional to the square root of its radius if the dome is composed of Bingham material. Such domes must therefore become relatively flatter as they enlarge. Moreover, a plot of dome height as a function of the square root of its radius must be a straight line that intersects the origin. The Bingham hypothesis consequently can be tested with height-radius data obtained during growth of a dome (cf. Fig. 9).

The major conceptual contrast between the model proposed here and the viscous and viscoplastic models is that the brittle-shell model treats the outer, cooled carapace of a lava dome as a material that is distinct from the ductile magma within the dome. Because the dome carapace is assumed to be under uniform tension, a magma (or gas) pressure in excess of hydrostatic pressure exists within the dome. This excess pressure balances the tensile stress in the carapace. Higher excess pressures require greater curvature, strength, or thickness of the carapace in order to balance the stresses. Consequently, if all other factors are constant, domes that are more nearly spherical can contain greater excess pressures and thus would be more prone to explosive failure than would relatively flatter domes. Quiescent failures (extrusions) would be more likely in flatter domes that have less surface curvature. Thus, the brittle-shell model is fundamentally different from previous models: it supposes a distinct mechanical behavior of the carapace, and it provides an explicit mechanism (tensile failure of the carapace) for eruptive dome growth, including both explosions and extrusions.

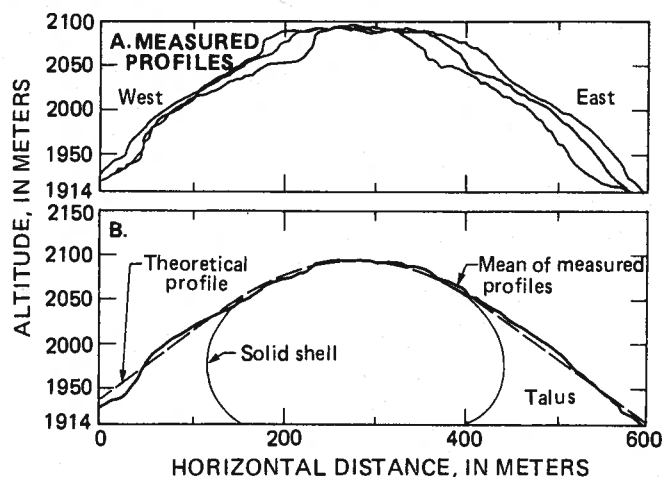


Fig. 5 *A, B.* Comparison of computed and measured topographic profiles of the Mount St. Helens lava dome. *A* Three profiles measured from a photogrammetric topographic map made from air photos taken on November 4, 1981. The three profiles are all roughly east-west, having azimuths of 73°, 91°, and 116° from due north, and each passes through the apex of the dome. The location of the upper margin of the talus apron is very difficult or impossible to distinguish in the field and is not useful as a modeling constraint. *B* The mean of the three measured profiles compared with a profile computed using "Halfdome". A *D* value of 1 and talus slopes of 36° were used in the computation

4.2 Comparison with Morphologic Data from Mount St. Helens

One means of testing model predictions with field data is to compare calculated dome profiles with those measured at Mount St. Helens (e.g., Swanson et al. 1987; Swanson and Holcomb 1987, and this Vol.). Such comparisons show excellent correspondence between predicted and measured cross-sectional profiles, particularly if the value of the single model parameter, *D*, is selected to maximize the goodness of fit (e.g., Fig. 5). However, it is important that the value of *D* is not selected through an exercise in unrestrained curve fitting. Table 1 shows that plausible values of *D* for the Mount St. Helens dome are of the order of one. The use of a *D* value of one to fit the curve of Fig. 5 is therefore physically reasonable.

As shown in Fig. 5, the correspondence between predicted and measured dome profiles is improved if several of the irregular, measured profiles are averaged to obtain a mean profile. For Mount St. Helens these mean profiles are best obtained by averaging several east-west profiles, because north-south profiles are asymmetrical owing to a pronounced south to north slope of the crater floor.

The close agreement between predicted and measured topographic profiles is perhaps surprising, in light of the complexity of dome growth as documented by Swanson et al. (1987). This documentation shows that the dome has grown partly by endogenous growth and partly by localized extrusions. Local extrusions impose local loads on the dome surface, which might be expected

Table 1. Plausible values of D and its constituent parameters for the Mount St. Helens dome

σ (Pa) ^a	t (m) ^b	γ (N/m ³) ^c	h (m)	D
1×10^7	10	26000	62	1
1×10^7	20	26000	44	2
1×10^7	30	26000	27	4
1×10^6	10	26000	20	1
1×10^6	20	26000	14	2
1×10^6	30	26000	11	3
1×10^6	10	26000	39	0.5
1×10^6	20	26000	55	0.5
1×10^6	30	26000	68	0.5

^a Estimates of the tensile strength of dome-carapace rock are based on typical crustal rock tensile strengths tabulated by Jaeger and Cook (1979, p. 190–191). Such tensile strengths vary by about one order of magnitude.

^b Estimates of the dome carapace thickness are based on preliminary analyses of magnetic data for the Mount St. Helens dome (personal communication, D. Dzurisin and R.P. Denlinger, U.S. Geological Survey).

^c The estimate of dome-rock unit weight is based on hundreds of measurements of Mount St. Helens dacite erupted in 1980 (personal communication, R.P. Hoblitt, U.S. Geological Survey).

to cause asymmetrical dome growth. However, the rock added to the dome surface during extrusions probably has about the same density as the magma inside the dome, and if the dome shell acts as a membrane, it should comply to the new load over a period of time so as to preserve the equilibrium dome configuration. Furthermore, the thickened dome shell that results from an extrusion will strengthen that part of the dome so that subsequent extrusions will tend to occur elsewhere. (This type of behavior has been documented at Mount St. Helens.) Thus, in an average sense, the equilibrium shape of the dome can be maintained even under the influence of local extrusions.

4.3 Comparison with Dome-Growth Data from Mount St. Helens

The brittle-shell model does not include explicit time dependence, and consequently it cannot predict rates of dome growth without independent knowledge of the rate of change of the parameters that compose D . Similar independent knowledge (of the rate of magma entry, for example) is necessary for *any* model to predict rates of dome growth. However, even without this independent knowledge, the brittle-shell model *can* predict how the dome shape and volume change during growth. That is, it can predict scenarios for how the ratios of dome height to volume, diameter to volume, and height to diameter change as the dome grows. These predictions can be compared with detailed data collected over a 6-year period at Mount St. Helens.

A complication in making theoretical predictions of height-volume and similar relations is that it is not known a priori which physical parameters change and which, if any, stay nearly the same during dome growth. That is, among the parameters that compose D (i.e., σ , t , γ , and h), one or more must change for dome growth to occur. For fixed values of these parameters, the dome can exist in only *one* equilibrium size and shape.

The simplest scenario for dome growth is that it occurs through compensating increases in σ , t , γ , and h , which cause D to remain roughly constant. Dome growth then occurs as self-similar expansion, and the dome shape remains roughly the same. During this self-similar growth, t and h are perhaps the parameters most likely to change, whereas σ and γ are more likely to remain almost constant.

Swanson and Holcomb (1987, and this Vol.) report that growth of the dacite dome at Mount St. Helens was approximately self-similar after May 1981. They measured dome heights and diameters on a series of detailed topographic maps and calculated volumes from digitized versions of the maps. The base of the dome was fixed at 1914 m elevation for all measurements and calculations. Swanson and Holcomb's best-fit, nonlinear regression equation for the height-volume data is

$$V = 657700 e^{0.019H} \quad (r^2 = 0.97) , \quad (15)$$

where V is the volume of the dome measured in cubic meters, and H is the height of the dome measured in meters. Their best-fit, nonlinear regression for the diameter-volume data is

$$V = 0.003 d^{3.494} \quad (r^2 = 0.99) , \quad (16)$$

where d is the diameter of the dome base measured in meters. Plots of these equations, along with the field data and theoretical predictions, are shown in Figs. 6 and 7.

Swanson and Holcomb (this Vol.) describe the errors implicit in the data plotted in Figs. 6 and 7. The errors in computed dome volumes arise principally from imperfect digital representation of the irregular dome surface, and may be as large as 10%. These errors must be borne in mind when deciding how many refinements of theory are justified in pursuing a good fit to the data.

The theoretical predictions of dome height-volume and diameter-volume relations shown in Figs. 6 and 7 are based on several scenarios for self-similar growth. Different scenarios employ different values of D and/or different assumptions about the extent of the talus apron that mantles the lower parts of the dome. For each scenario, however, the basic strategies used to calculate the theoretical dome volume are the same.

Two methods exist for calculating the theoretical volume enclosed by the brittle dome carapace. The first method relies on "Halfdome" and uses numerical integration to compute the volume above any selected horizontal plane that transects the dome (Appendix 1). The second method is useful only

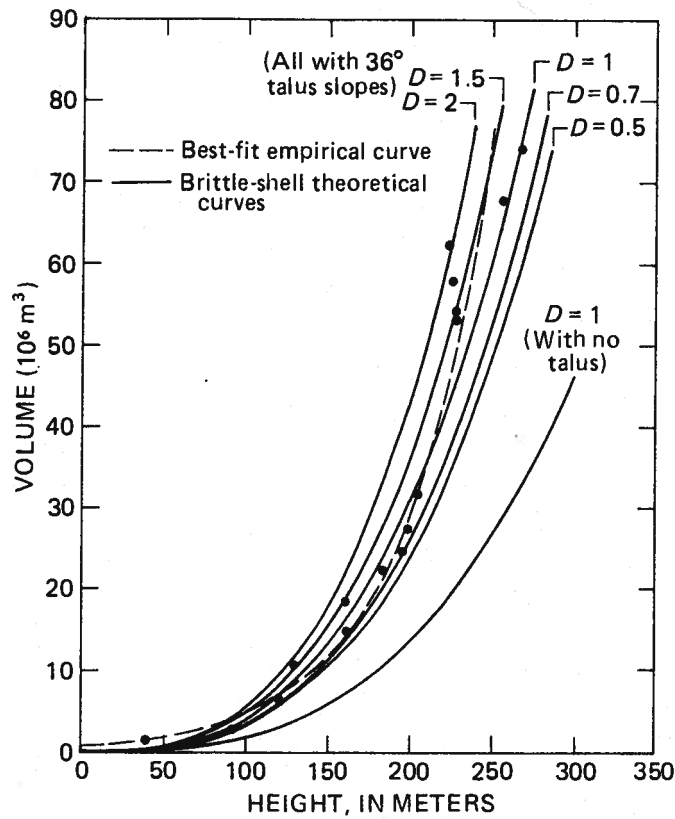


Fig. 6. Lava dome volume as a function of height. Data points are from measurements of the Mount St. Helens dome by Swanson and Holcomb (this Vol.), and the *dashed line* is the empirical, exponential curve that best fits the data. The *solid lines* represent theoretical results for five self-similar dome growth scenarios. Swanson and Holcomb (this Vol.) report that dome growth was approximately self-similar after May 1981, when the dome was about 130 m high. The theoretical curves were obtained from numerical simulations using "Halfdome"

for determining the *total* volume enclosed by the carapace. This method exploits the balance of forces that act on the base of the carapace, which has a radius R_2 (Fig. 8). The magma pressure on the base is equal to $(h+H)\gamma$, where h is the pressure head at the apex of the dome and H is the height of the apex above the base (Fig. 8). Multiplying this magma pressure by the area of the base, πR_2^2 , gives an expression for the total vertical force on the base. An additional expression for the total vertical force is given by the product of the dome volume, V , and the unit weight of the dome, γ . Equating these two expressions for the vertical force and dividing each by γ gives an equation by which to find the dome volume enclosed by the brittle carapace:

$$V = \pi R_2^2 (H+h) . \quad (17)$$

This equation, which fortuitously has the same, simple form as the equation for a right, circular cylinder, provides a means for checking the accuracy of the numerical calculation of the dome's volume. However, if a talus apron is to be included in the calculation of the total dome volume, Eq. (17) serves no useful purpose.

To include bordering talus in the volume calculation, the volume of the part of the dome above the talus apron and having thickness H_1 (Fig. 8) is ob-

Fig. 7. Lava dome volume as a function of the base diameter. Data points are from measurements of the Mount St. Helens dome by Swanson and Holcomb (this Vol.), and the dashed line is the empirical, power-law curve that best fits the data. The solid lines represent theoretical results for five self-similar dome growth scenarios. (Two scenarios produce nearly identical curves.) The theoretical curves were obtained from numerical simulations using "Halfdome"

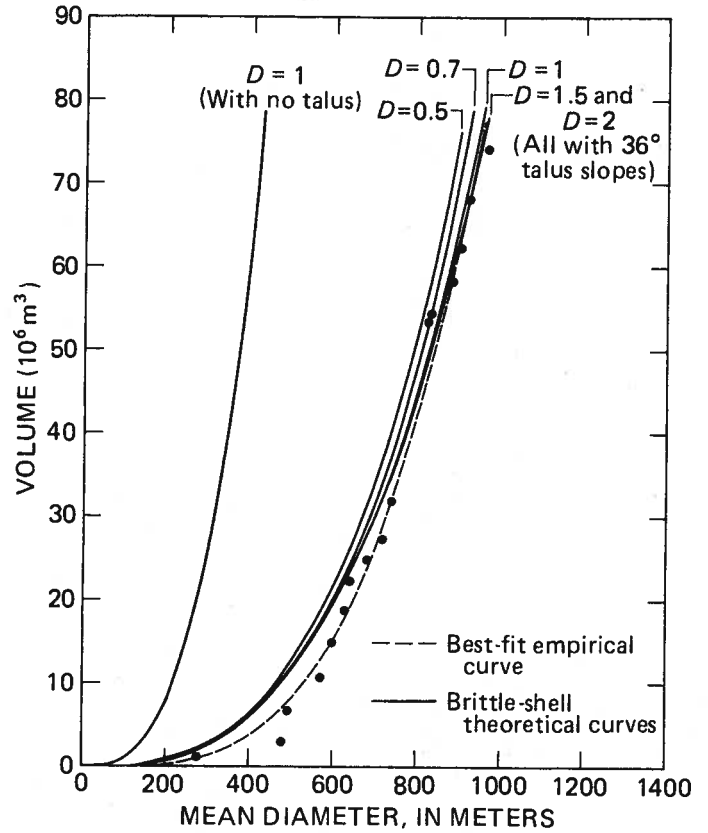
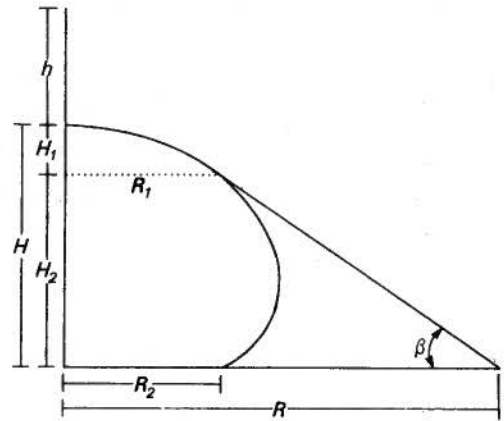


Fig. 8. Definition sketch of a cross-section of half a lava dome, showing the geometric parameters used in computing theoretical dome volumes



tained from numerical integration using "Halfdome." Designate this volume V_1 . Below H_1 the volume of the dome is approximated as that of a right conic frustrum. The sloping surface of the conic frustrum is the surface of the talus apron, and the volume of the frustrum is given by (Tuma 1979, p. 27)

$$V_2 = \frac{\pi H_2}{3} (R_1^2 + RR_1 + R^2) , \quad (18)$$

where V_2 is the volume of the part of the dome below the upper margin of the talus, H_2 is the height of the talus apron above the dome base (i.e., the height of the frustrum), R_1 is the radius of the dome at height H_2 , and R is the radius of the dome base (Fig. 8). If the surface of the talus apron slopes at a uniform angle β , then H_2 , R , and R_1 are related by the simple geometric equation

$$H_2 = (R - R_1) \tan \beta . \quad (19)$$

The total volume of the dome plus talus apron is found by adding Eq. (18) to V_1 , making use of Eq. (19) if desired:

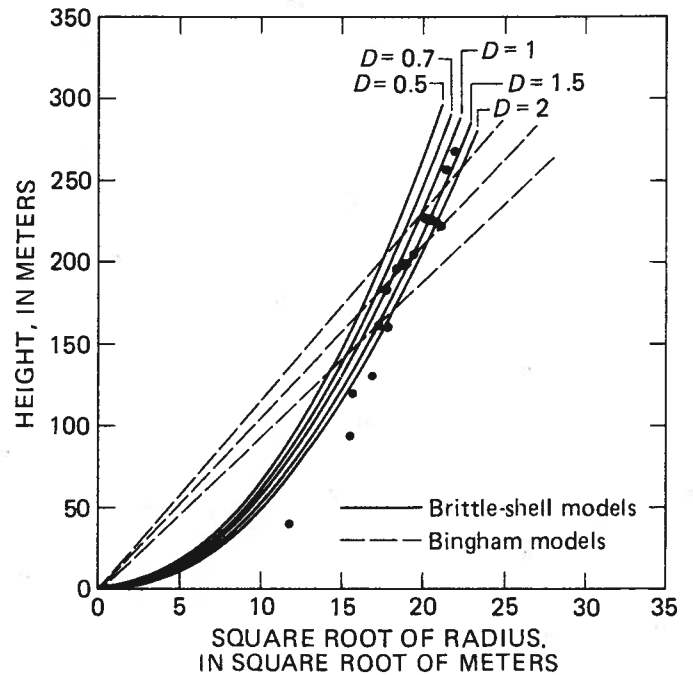
$$V = V_1 + V_2 = V_1 + \frac{\pi(R - R_1) \tan \beta}{3} (R_1^2 + RR_1 + R^2) . \quad (20)$$

Inserting appropriate values for the geometric parameters in Eq. (20) allows theoretical predictions of dome height-volume and diameter-volume relations to be compared with field data. Each point on the theoretical curves of Figs. 6 and 7 was obtained by extracting the necessary values from numerical simulation results generated using "Halfdome". For the curves that include talus aprons in the computed dome volumes, the angle of the talus slopes was fixed at 36° . On the basis of several measurements made on each of seven topographic maps of the Mount St. Helens dome (R. T. Holcomb and D. A. Swanson, U.S. Geological Survey, unpublished data), $36^\circ \pm 5^\circ$ is a reasonable estimate of the mean talus slope angle.

Figures 6 and 7 show that the best match of the theoretical curves to the field data is generated if the D value is about one and the 36° talus apron is included in the dome volume. This scenario does not provide the best match to both the volume-height and volume-diameter data, but it provides the best compromise in simultaneously fitting both types of data. The deviation of the best-fit theoretical curves from most of the field data is negligible if the possibility of 10% error in the data is taken into account.

For dome diameters less than about 750 m, however, the deviation of the theoretical curves from the diameter-volume data is systematic and significant (Fig. 7). In such instances the theory overestimates the volume of the dome. This systematic deviation reflects at least two phenomena. First, during early stages of growth of the Mount St. Helens dome, the dome was somewhat more asymmetrical than during later stages (Swanson and Holcomb, this Vol.). The theory uses the mean dome diameter as the basis for volume calculations, and consequently it systematically overestimates the volume when the dome is significantly asymmetrical. Second, the dome did not grow in a self-similar fashion until its mean diameter reached nearly 600 m (Swanson and Holcomb,

Fig. 9. Comparison of Bingham models and brittle-shell models for predicting dome height as a function of the square root of radius. Data points are the same as those plotted in Figs. 6 and 7



this Vol.). Thus, the self-similar growth curves cannot be expected to predict the data for smaller domes with great accuracy.

Another means of assessing self-similar growth predictions entails plotting dome height as a function of the square root of its radius. This permits a straightforward comparison of the Bingham and brittle-shell hypotheses. Predictions based on the brittle-shell theory are plotted on Fig. 9, along with the pertinent data. The Bingham-model prediction described by Blake (1987, and this Vol.) plots as a straight line that passes through the origin of Fig. 9. The slope of the line is determined by the yield strength and density of the dome's lava. Neither the Bingham nor the brittle-shell theory fits all the data, but the inaccuracy of the brittle-shell theory is negligible except for cases in which the dome was less than 150 m in height. For these cases growth of the dome was not self-similar.

Some alternative hypotheses for lava-dome growth make use of the brittle-shell model but not of the self-similar growth concept. Instead, such hypotheses suppose that D changes during dome growth. A scenario of this type that seems quite plausible is one in which the thickness of the dome carapace, t , increases during growth, while the other parameters that contribute to D remain more or less constant. In this case the basic dome-shape equation (17) can be scaled against the value of h , which is assumed constant, and Eq. (17) can be reduced to a dimensionless form:

$$\frac{V}{h^3} = \pi \frac{[R_2(D)]^2}{h^2} [H(D)/h + 1] . \quad (21)$$

Here, R_2 and H are both functions of D that need to be obtained from numerical solutions using "Halfdome". The disadvantage of this type of hypothesis is that it involves more than one free parameter. That is, it allows the dome shape to change as the dome enlarges, with no independent constraints imposed by physical data. Thus, in the absence of additional information, matching the theory to the data becomes a relatively unrestrained exercise in curve-fitting. It therefore yields a rather small increment of physical insight, and the topic is not pursued here.

5 Conclusions and Unresolved Questions

This chapter describes a brittle-shell model for lava domes that is conceptually simple, quantitatively explicit, and computationally economical. The model results constitute a testable hypothesis for the mechanical controls of lava-dome morphology and growth.

The brittle-shell model differs significantly from previous mechanical models of lava domes. The primary difference is the presumption that the solid rock composing the outer carapace of the dome has mechanical properties that differ markedly from those of the molten rock within the dome. The important properties of the outer carapace are its tensile strength and thickness, whereas the important properties of the molten interior are its pressurization and weight. A single dimensionless number, D , represents the combined effect of these four properties, and its value determines the shape of the dome. Talus slopes that mantle the lower parts of the dome are assumed to contribute only cosmetically, and not mechanically, to its shape.

An important feature of the brittle-shell model is that it provides conceptually for a means of eruptive lava-dome growth. The dome can grow through tensile failure of its outer shell. Alternatively, endogenous dome growth can occur if changes in the dome-shell thickness or strength keep pace with pressurization in the feeding conduit, which causes intrusion of new magma into the dome interior.

The brittle-shell model also adequately matches morphologic data obtained for the growing Mount St. Helens dome. Plots of dome volume as a function of its diameter and height and of height as a function of radius reflect the shape of the dome and how it might change during growth. The match between theoretical predictions and the data is best if a scenario of self-similar-dome growth is assumed with D always equal to about one. A D value of the order of one is commensurable with estimates of the strength, shell thickness, unit weight, and pressurization of the Mount St. Helens dome. Moreover, a D value of one produces a good match of theoretical and measured topographic profiles for the Mount St. Helens dome.

A more rigorous test of the brittle-shell hypothesis would require independent measurement of each of the parameters that contribute to D . The most poorly constrained parameters appear to be the thickness of the solid dome carapace and the pressure of the fluid phase within the dome. Future research

that included drilling into the dome's interior therefore could provide valuable data to test the applicability of the brittle-shell hypothesis.

Other future research could be directed toward making the brittle-shell model more realistic by allowing for tensile stress and strength heterogeneities in the mathematical formulation. Moreover, research on the rate-dependent processes by which the dome shell may fracture and grow expands the ramifications of the model and addresses the processes that act during disequilibrium states. Such research is described by Denlinger (this Vol.).

Acknowledgments. I thank the many CVO staff members, and particularly Don Swanson, who collected the extraordinary data set on the Mount St. Helens dome. Chuyler Freeman assisted with construction of topographic profiles, and Rick LaHusen provided advice on making "Halfdome" user-friendly. Don Swanson, Roger Denlinger, and David Pollard provided thoughtful critiques of the manuscript.

Appendix 1: Computer Program Halfdome

The computer program "Halfdome" takes about a minute to compute and plot a solution of the system (11, 12, 14a, b) if an IBM XT¹-type personal computer with CGA graphics is used and the program is accessed through the hard disk. An option when using "Halfdome" is to include a bordering talus apron adjacent to the side of the dome. The presence of the talus apron does not affect the procedure for solving the equations; the talus only contributes cosmetically to the shape of the dome.

A file output by "Halfdome", which has a default name of "Dome.dat", lists the cumulative volume computed as the numerical integration proceeds from the apex to the base of the dome carapace. The partial dome volume lying above a horizontal plane that transects the carapace at an arbitrary elevation may therefore be read directly from "Dome.dat". The final entry in "Dome.dat" is the total volume enclosed by the dome carapace.

```

10 REM*****
20 REM                HALFDOME.Bas
30 REM                (R.M. Iverson 7/6/87)
40 REM*****
50 REM This program computes the profile of half of a lava dome by numerical
60 REM solution of two simultaneous, nonlinear, ordinary differential
65 REM equations that have their basis in the following physical assumptions:
70 REM 1. At any moment in time, the dome is in static mechanical equilibrium.
80 REM 2. The dome consists of a pressurized magma body enclosed by a carapace
90 REM    of solid rock. The carapace is assumed to be of uniform thickness
100 REM    and tensile strength. The carapace, in turn, is surrounded along its
110 REM    lower margins by an apron of talus that is assumed to be in plastic
120 REM    equilibrium. Thus the talus contributes no strength to help support
130 REM    the dome.
140 REM 3. The physical parameters that determine the shape of the dome are
150 REM    the magma pressure (expressed as head) at the apex of the dome,

```

¹ The use of brand and trade names in this chapter is for identification purposes only and does not constitute endorsement by the U.S. Geological Survey.

```

160 REM      the magma density (expressed as unit weight), which is assumed to be
170 REM      constant, the tensile strength of the solid rock carapace,
175 REM      and the thickness of the carapace. These parameters are combined
180 REM      into one dimensionless parameter, D, that characterizes the forces
190 REM      that determine the shape of the dome. D is the only free parameter
200 REM      that affects the numerical solution of the governing equations.
210 REM*****
215 REM
220 REM To run the program, enter the BASIC interpreter program, type load
230 REM "Halfdome", and then type run. The program will first prompt for the
240 REM name of a file into which numeric output data are placed, and then will
245 REM prompt for the desired value of D, for the desired angle of the
250 REM bordering talus slope, and for a scale factor that determines the size
260 REM of the graphic output on the monitor screen.
270 REM
280 REM*****
290 REM
300 REM DEFINITION OF VARIABLES:
310 REM D - A dimensionless number that incorporates the effects of magma pres-
320 REM sure and density, and of dome-carapace thickness and tensile strength.
325 REM Rho - A dimensionless horizontal coordinate of a point on the dome
330 REM surface. The origin for Rho is at the axis of the dome.
340 REM Xi - A dimensionless vertical coordinate of a point on the dome surface.
345 REM The origin for Xi is at a distance h above the dome apex, where
350 REM h is the pressure head at the apex.
360 REM Eta - A number equal to the sine of the dome-surface slope.
370 REM Mu - A number equal to the cosine of the dome-surface slope.
380 REM COUNT - A counter to keep track of which of three segments of the
390 REM dome profile is being calculated.
400 REM N and NN - Iterative indices for loop procedures.
410 REM STP - Size of the space step used in the numerical solution
420 REM SCALE - A number which gives the linear scale of the solution plotted
430 REM on the graphics monitor. The number is relative only and has no
440 REM particular physical meaning or importance.
450 REM RHOPILOT - Value of rho scaled appropriately for graphic plotting.
460 REM XIPILOT - Value of XI scaled appropriately for graphic plotting.
470 REM OLDRHO - Value of Rho saved from previous numerical step
480 REM OLDXI - Value of XI saved from previous numerical step
490 REM ORHOPILO - Value of OLDRHO scaled for graphics use
500 REM OXIPILO - Value of OLDXI scaled for graphics use
510 REM TALUSLOPE - User-specified slope angle (in degrees) of the talus apron
520 REM surrounding the base of the dome
530 REM RHOTALUS - Value of RHO where the talus apron adjoins the dome
540 REM XITALUS - Value of XI where the talus apron adjoins the dome
550 REM RHOTALUSPLO - Value of RHOTALUS scaled for graphics use
560 REM XITALUSPLO - Value of XITALUS scaled for graphics use
570 REM TALUSADJOIN - Slope angle (in degrees) at the spot on the dome where
580 REM the adjoining talus slope contacts the dome. If no talus slope is
590 REM specified, then this parameter defines the slope of the dome at the
600 REM point where the dome contacts the horizontal dome base.
610 REM TALUSAPRON - If this parameter = 0, then no talus slope is specified
620 REM to apron the dome. If this parameter = 1, then a talus apron exists
630 REM TESTANGLE - This angle is used to test the calculated dome slope
640 REM against the angle specified for TALUSADJOIN
650 REM VOLSUM - Cumulative sum of the dome volume above current Xi
660 REM*****
670 REM
680 REM***** BEGIN EXECUTABLE PART OF PROGRAM*****
685 REM
690 REM*****
700 REM PROMPT USER FOR NAME OF NUMERIC OUTPUT FILE
710 CLS:PRINT:PRINT:PRINT"DOME PROFILE PROGRAM"
720 PRINT:INPUT"Enter filename for numeric output (Default = Dome.dat)";NF$
730 IF NF$="" THEN NF$="DOME.DAT"
740 OPEN NF$ FOR OUTPUT AS 1
750 REM SPECIFY N AND C AS INTEGER-VARIABLE MARKERS
760 DEFINT N,C
770 REM PROMPT FOR THE VALUE OF THE PARAMETER D (=a/h)
780 PRINT:PRINT "The D parameter should be 0.5 < D < 20"
790 INPUT "Enter the value of the parameter D";D
800 REM PROMPT FOR USER SELECTION (YES OR NO) OF TALUS APRON AROUND DOME
810 PRINT " "
820 PRINT "Is a talus apron around the dome desired? Enter 0 (zero) if
830 INPUT "no apron is desired and 1 if it is desired"; TALUSAPRON

```

```

840 REM PROMPT FOR USER SELECTION OF TALUSADJOIN ANGLE
850 PRINT:PRINT "If no talus apron was specified, now enter as TALUSADJOIN"
860 PRINT "the angle of the dome surface where it contacts the dome base."
870 PRINT "Otherwise, TALUSADJOIN specifies the slope angle (in degrees)"
880 PRINT "of the point on the dome where talus adjoins the dome surface."
890 INPUT "Enter TALUSADJOIN value in degrees (between 15&90)";TALUSADJOIN
900 REM PROMPT USER FOR THE ANGLE OF THE TALUS SLOPE, IF SLOPE IS SPECIFIED
910 PRINT:PRINT "The TALUSLOPE parameter specifies the angle of the talus"
920 PRINT "apron adjoining the dome, ranging from 15 to 90 degrees"
930 INPUT "Enter TALUSLOPE value in degrees (Default is 35)";TALUSLOPE
940 REM SET DEFAULT VALUES OF PARAMETERS
950 IF TALUSLOPE=0 THEN TALUSLOPE=35
960 IF TALUSADJOIN=0, THEN TALUSADJOIN=35
970 TALUSLOPE=TALUSLOPE*.0174533
980 TALUSADJOIN=TALUSADJOIN*.0174533
990 IF D=0 THEN D=4
1000 REM SPECIFY THE SIZE OF THE SPACE STEP FOR THE NUMERICAL SOLUTION
1010 STP=.01
1020 REM PROMPT FOR THE "SCALE" FACTOR TO DETERMINE THE SIZE OF THE PLOT
1030 PRINT:PRINT "The scale of the plotted output is set by specifying SCALE"
1040 PRINT "The default value of SCALE is 50"
1050 INPUT "Enter the value of SCALE"; SCALE
1060 IF SCALE=0, THEN SCALE=50
1070 REM FIX VALUES OF Rho, Eta, Xi, AND Volsum AT THE APEX OF THE DOME
1080 RHO=0
1090 ETA=0
1100 VOLSUM=0
1110 XI=1/D
1120 REM PRINT HEADINGS AND THE DATA VALUES FOR THE DOME APEX TO OUTPUT FILE
1130 PRINT#1, "Rho Xi Eta Volume Sum"
1140 PRINT #1, RHO,XI,ETA,VOLSUM
1150 REM CLEAR THE MONITOR AND PREPARE FOR GRAPHICS OUTPUT
1160 CLS
1170 SCREEN 2
1180 KEY OFF
1190 REM DRAW A VERTICAL LINE OF LENGTH h/a (=1/D) ATOP THE DOME APEX
1200 RHOPLOT=0
1210 XIPILOT=XI*SCALE+20
1220 LINE(0,20)-(RHOPLOT,XIPILOT)
1230 REM RETAIN THE CURRENT RHO VALUE FOR FUTURE USE
1240 OLDRHO=RHO
1250 REM*****
1260 REM
1270 REM***** BEGIN COMPUTATION OF DOME PROFILE *****
1280 REM (THIS ROUTINE IS USED TWICE TO COMPUTE THE FLATTER PARTS OF THE
1290 REM DOME PROFILE. Rho IS THE INDEPENDENT VARIABLE IN THIS CALCULATION)
1300 REM*****
1310 REM
1320 COUNT=0
1330 REM ANALYTICALLY CALCULATE THE VALUE OF Eta ONE STEP FROM THE ORIGIN
1340 RHO=RHO+STP
1350 ETA=.5 * (1/D) * RHO
1360 REM BEGIN LOOP TO CALCULATE THE REST OF THE DOME PROFILE, STEPPING
1370 REM OUTWARD AND DOWNWARD FROM THE APEX OF THE DOME
1380 FOR N = 1 TO 500
1390 IF COUNT=1, THEN IF N=1, THEN GOTO 1530
1400 OLDXI=XI
1410 IF COUNT=0, THEN XI=XI+STP*(ETA/SQR(1-ETA*ETA))
1420 IF COUNT=1, THEN XI=XI-STP*(ETA/SQR(1-ETA*ETA))
1430 VOLSUM=VOLSUM + (XI-OLDXI)*3.14159*((RHO+OLDRHO)/2)^2
1440 REM PRINT CURRENT VALUES OF RHO, XI, ETA, AND VOLSUM TO OUTPUT FILE
1450 PRINT #1, RHO,XI,ETA,VOLSUM
1460 REM PLOT A LINE CONNECTING TWO ADJACENT POINTS ON THE DOME PROFILE
1470 ORHOPLO=2.02*OLDRHO*SCALE
1480 OXIPILO=OLDXI*SCALE+20
1490 RHOPLOT=2.02*RHO*SCALE
1500 XIPILOT=XI*SCALE+20
1510 LINE(ORHOPLO,OXIPILO)-(RHOPLOT,XIPILOT)
1520 REM USE RUNGE-KUTTA ALGORITHM TO CALCULATE Eta FOR THE NEXT STEP
1530 AN=STP*(XI-ETA/RHO)
1540 BN=STP*(XI-(ETA+AN/2)/(RHO+STP/2))
1550 CN=STP*(XI-(ETA+BN/2)/(RHO+STP/2))
1560 DN=STP*(XI-(ETA+CN)/(RHO+STP))
1570 ETA=ETA+(1/6)*(AN+2*(BN+CN)+DN)

```

```

1580 REM STORE AND INCREMENT THE VALUE OF Rho
1590   OLDRHO=RHO
1600   RHO=RHO+STP
1610 REM TEST SLOPE ANGLE FOR MATCH WITH TALUSLOPE ANGLE
1620   TESTANGLE = ETA - SIN(TALUSADJOIN)
1630   IF COUNT=0, THEN IF ETA>.25, THEN IF ABS(TESTANGLE)<=.01, THEN GOTO 1650
1640   GOTO 1700
1650   RHOTALUS=RHO
1660   XITALUS=XI
1670 REM IF THERE IS NO TALUS APRON AND THE BASE SLOPE IS REACHED, GOTO END
1680   IF TALUSAPRON=0, THEN GOTO 2370
1690 REM TEST FOR 50-DEGREE SLOPE TO ENACT ALGORITHM SWITCH
1700   IF ETA>=.776, THEN GOTO 1830
1710   IF COUNT=1, THEN IF ETA<.01, THEN COUNT=2
1720   IF COUNT=2, THEN GOTO 2370
1730   NEXT N
1740   IF COUNT=2 GOTO 1080
1750   IF N=500, THEN STOP
1760 REM*****
1770 REM
1780 REM BEGIN CALCULATION OF THE STEEP PART OF THE DOME PROFILE,
1790 REM SWITCHING TO AN ALGORITHM USING Xi AS THE INDEPENDENT VARIABLE
1800 REM AND INTRODUCING Mu AS A DEPENDENT VARIABLE
1810 REM
1820 REM*****
1830   MU=SQR(1-ETA*ETA)
1840   OLDRHO=RHO
1850   OLDXI=XI
1860 REM BEGIN LOOP TO CALCULATE THE STEEP PART OF THE DOME PROFILE
1870   FOR NN = 1 TO 500
1880   REM USE RUNGE-KUTTA ALGORITHM TO CALCULATE Mu FOR THE NEXT STEP
1890   AN=STP*((SQR(1-MU*MU)/RHO)-XI)
1900   BN=STP*((SQR(1-(MU+.5*AN))*(MU+.5*AN))/RHO)-(XI+.5*STP)
1910   CN=STP*((SQR(1-(MU+.5*BN))*(MU+.5*BN))/RHO)-(XI+.5*STP)
1920   DN=STP*((SQR(1-(MU+.5*CN))*(MU+.5*CN))/RHO)-(XI+STP)
1930   MU=MU+(1/6)*(AN+2*(BN+CN)+DN)
1940 REM CALCULATE Rho FOR THIS STEP
1950   RHO=RHO+STP*(MU/SQR(1-MU*MU))
1960 REM CALCULATE Eta
1970   ETA=SQR(1-MU*MU)
1980 REM*****
1990 REM THE NEXT NINE LINES LOCATE THE POSITION OF THE TOP OF THE TALUS SLOPE
1995 REM*****
2000 REM TEST FOR SLOPE ANGLE MATCH WITH TALUSADJOIN ANGLE
2010   IF RHO<=OLDRHO, THEN GOTO 2100
2020   TESTANGLE=ETA-SIN(TALUSADJOIN)
2030   IF ABS(TESTANGLE)<=.01, THEN GOTO 2050
2040   GOTO 2100
2050   RHOTALUS=RHO
2060   XITALUS=XI
2070   IF TALUSAPRON=0, THEN GOTO 2370
2080 REM*****
2090 REM INCREMENT THE VALUE OF Xi
2100   XI = XI + STP
2110   VOLSUM = VOLSUM + (XI-OLDXI)*3.14159*((RHO+OLDRHO)/2)^2
2120 REM PRINT NEW VALUES OF Rho, Xi, Eta, AND Volsum
2130   PRINT #1, RHO,XI,ETA,VOLSUM
2140 REM PLOT Rho AND Xi
2150   ORHOPLO=2.02*RHO*SCALE
2160   OXIPLO=OLDXI*SCALE+20
2170   RHOPLOT=2.02*RHO*SCALE
2180   XIPLT=XI*SCALE+20
2190   LINE(ORHOPLO,OXIPLO)-(RHOPLOT,XIPLT)
2200 REM STORE THE CURRENT VALUES OF Rho AND Xi FOR LATER USE
2210   OLDRHO=RHO
2220   OLDXI=XI
2230 REM TEST FOR 140-DEGREE SLOPE TO ENACT ALGORITHM SWITCH
2240   IF NN=500, THEN STOP
2250   IF MU<=-.766, THEN GOTO 2280
2260   NEXT NN
2270 REM EXIT THIS ROUTINE AND RESUME CALCULATION WITH Rho INDEP. VAR.
2280   STP=-STP
2290   COUNT=1
2300   GOTO 1380

```

```

2310 REM*****
2320 REM
2330 REM***** PERFORM CALCULATIONS TO FINISH THE PLOT *****
2340 REM          BY ADDING THE TALUS SLOPE AND DOME BASE
2350 REM*****
2360 REM CALCULATE LOCATIONS OF TOP AND BASE OF THE MARGINAL TALUS SLOPE
2370   RHOTALUSPLO=RHOTALUS*2.02*SCALE
2380   XITALUSPLO=XITALUS*SCALE+20
2390   XPLOT = (XIPLLOT-XITALUSPLO)/(TAN(TALUSLOPE)/2.02)+RHOTALUSPLO
2400 REM DRAW LINES TO DEMARCATE THE MARGINAL TALUS SLOPE
2410   LINE(RHOTALUSPLO,XITALUSPLO)-(XPLOT,XIPLLOT)
2420   LINE(XPLOT,XIPLLOT)-(0,XIPLLOT)

```

References

- Bates RL, Jackson JA (eds) (1980) Glossary of geology, Falls Church, Va. American Geological Institute
- Blake S (1987) Modeling lava domes as Bingham fluids (abs.). International Union of Geodesy and Geophysics, XIX General Assembly, Abstracts vol 2
- Denlinger RP (1987) An analysis of dome-building eruptions as creep-rupture phenomena (abs.). International Union of Geodesy and Geophysics, XIX General Assembly, Abstracts vol 2:413
- Flügge W (1967) Stresses in shells. Springer, Berlin Heidelberg New York
- Goetze C (1971) High temperature rheology of Westerly granite. *J Geophys Res* 76: 1223-1230
- Huppert HE, Shepherd JB, Sigurdsson H, Sparks RSJ (1982) On lava dome growth, with application to the 1979 lava extrusion of the Soufriere of St. Vincent. *J Volcanol Geotherm Res* 14:199-222
- Jaeger JC, Cook NWG (1979) Fundamentals of rock mechanics, 3rd edn. Chapman and Hall, London
- Kreyszig E (1979) Advanced engineering mathematics, 4th edn. Wiley, New York
- Swanson DA, Holcomb RT (1987) General consistencies in the growth of the Mount St. Helens lava dome, 1980-86 (abs.). International Union of Geodesy and Geophysics, XIX General Assembly, Abstracts vol 2:412
- Swanson DA, Dzurisin D, Holcomb RT, Iwatsubo EY, Chadwick WW, Casadevall TJ, Ewert JW, Heliker CC (1987) Growth of the lava dome at Mount St. Helens, Washington, (USA) In: Fink JH (ed) *GSA Spec Pap* 212:1-16
- Tuma JJ (1979) Engineering mathematics handbook, 2nd edn. McGraw Hill, New York